

Lamin A/C dysregulation contributes to cardiac pathology in a mouse model of severe spinal muscular atrophy.

| | |
|-------------------------------|--|
| Journal: | <i>Human Molecular Genetics</i> |
| Manuscript ID | HMG-2019-D-00455.R1 |
| Manuscript Type: | 2 General Article - UK Office |
| Date Submitted by the Author: | n/a |
| Complete List of Authors: | <p>Šoltić, Darija; Keele University, Institute for Science and Technology in Medicine; Robert Jones and Agnes Hunt Orthopaedic and District Hospital NHS Trust, Wolfson Centre for Inherited Neuromuscular Disease Shorrock, Hannah; University of Edinburgh, Centre for Discovery Brain Sciences</p> <p>Allardyce , Hazel; University of Aberdeen, Institute of Education for Medical and Dental Science, College of Medicine</p> <p>Wilson, Emma; University of Chester, Chester Medical School</p> <p>Holt, Ian; Robert Jones and Agnes Hunt Orthopaedic and District Hospital NHS Trust, Wolfson Centre for Inherited Neuromuscular Disease</p> <p>Synowsky, Silvia; University of St Andrews, 6BSRC Mass Spectrometry and Proteomics Facility</p> <p>Shirran, Sally; University of St Andrews, BSRC Mass Spectrometry and Proteomics Facility</p> <p>Parson, Simon; University of Aberdeen, Institute of Education for Medical and Dental Science, College of Medicine, Medical Sciences and Nutrition</p> <p>Gillingwater, Thomas; University of Edinburgh, Euan MacDonald Centre for Motor Neurone Disease Research</p> <p>Fuller, Heidi; Keele University, Institute for Science and Technology in Medicine; Robert Jones and Agnes Hunt Orthopaedic and District Hospital NHS Trust, Wolfson Centre for Inherited Neuromuscular Disease</p> |
| Key Words: | spinal muscular atrophy, SMA, Lamin A/C, Heart, Proteomics |
| | |

1
2
3
4 **Lamin A/C dysregulation contributes to cardiac pathology in a**
5
6 **mouse model of severe spinal muscular atrophy**
7
8
9

10
11 Darija Šoltić^{1,2}, Hannah K Shorrocks³, Hazel Allardyce⁴, Emma L Wilson⁵, Ian Holt², Silvia A
12
13 Synowsky⁶, Sally L Shirran⁶, Simon H Parson⁴, Thomas H Gillingwater³, Heidi R Fuller^{1,2*}
14
15

16
17
18 ¹Institute for Science and Technology in Medicine, Keele University, Keele ST5 5BG, UK;

19
20 ²Wolfson Centre for Inherited Neuromuscular Disease, TORCH Building, RJA Orthopaedic
21
22 Hospital, Oswestry SY10 7AG, UK; ³Edinburgh Medical School: Biomedical Sciences,
23
24 University of Edinburgh, UK; Euan MacDonald Centre for Motor Neurone Disease Research,
25
26 University of Edinburgh, Edinburgh EH8 9XD, UK; ⁴Institute of Education for Medical and
27
28 Dental Science, College of Medicine, Medical Sciences and Nutrition, University of
29
30 Aberdeen AB24 3FX, UK; ⁵Chester Medical School, University of Chester, Chester CH1
31
32 4BJ, UK; ⁶BSRC Mass Spectrometry and Proteomics Facility, University of St Andrews, St
33
34 Andrews KY16 9ST, UK.
35
36
37
38
39
40
41
42

43
44
45
46
47
48
49
50
51
52
53 *Corresponding author

54
55
56
57
58
59
60
61
62
63
64
65
66
67
68
69
70
71
72
73
74
75
76
77
78
79
80
81
82
83
84
85
86
87
88
89
90
91
92
93
94
95
96
97
98
99
100
101
102
103
104
105
106
107
108
109
110
111
112
113
114
115
116
117
118
119
120
121
122
123
124
125
126
127
128
129
130
131
132
133
134
135
136
137
138
139
140
141
142
143
144
145
146
147
148
149
150
151
152
153
154
155
156
157
158
159
160
161
162
163
164
165
166
167
168
169
170
171
172
173
174
175
176
177
178
179
180
181
182
183
184
185
186
187
188
189
190
191
192
193
194
195
196
197
198
199
200
201
202
203
204
205
206
207
208
209
210
211
212
213
214
215
216
217
218
219
220
221
222
223
224
225
226
227
228
229
230
231
232
233
234
235
236
237
238
239
240
241
242
243
244
245
246
247
248
249
250
251
252
253
254
255
256
257
258
259
260
261
262
263
264
265
266
267
268
269
270
271
272
273
274
275
276
277
278
279
280
281
282
283
284
285
286
287
288
289
290
291
292
293
294
295
296
297
298
299
300
301
302
303
304
305
306
307
308
309
310
311
312
313
314
315
316
317
318
319
320
321
322
323
324
325
326
327
328
329
330
331
332
333
334
335
336
337
338
339
340
341
342
343
344
345
346
347
348
349
350
351
352
353
354
355
356
357
358
359
360
361
362
363
364
365
366
367
368
369
370
371
372
373
374
375
376
377
378
379
380
381
382
383
384
385
386
387
388
389
390
391
392
393
394
395
396
397
398
399
400
401
402
403
404
405
406
407
408
409
410
411
412
413
414
415
416
417
418
419
420
421
422
423
424
425
426
427
428
429
430
431
432
433
434
435
436
437
438
439
440
441
442
443
444
445
446
447
448
449
450
451
452
453
454
455
456
457
458
459
460
461
462
463
464
465
466
467
468
469
470
471
472
473
474
475
476
477
478
479
480
481
482
483
484
485
486
487
488
489
490
491
492
493
494
495
496
497
498
499
500
501
502
503
504
505
506
507
508
509
510
511
512
513
514
515
516
517
518
519
520
521
522
523
524
525
526
527
528
529
530
531
532
533
534
535
536
537
538
539
540
541
542
543
544
545
546
547
548
549
550
551
552
553
554
555
556
557
558
559
560
561
562
563
564
565
566
567
568
569
570
571
572
573
574
575
576
577
578
579
580
581
582
583
584
585
586
587
588
589
590
591
592
593
594
595
596
597
598
599
600
601
602
603
604
605
606
607
608
609
610
611
612
613
614
615
616
617
618
619
620
621
622
623
624
625
626
627
628
629
630
631
632
633
634
635
636
637
638
639
640
641
642
643
644
645
646
647
648
649
650
651
652
653
654
655
656
657
658
659
660
661
662
663
664
665
666
667
668
669
670
671
672
673
674
675
676
677
678
679
680
681
682
683
684
685
686
687
688
689
690
691
692
693
694
695
696
697
698
699
700
701
702
703
704
705
706
707
708
709
710
711
712
713
714
715
716
717
718
719
720
721
722
723
724
725
726
727
728
729
730
731
732
733
734
735
736
737
738
739
740
741
742
743
744
745
746
747
748
749
750
751
752
753
754
755
756
757
758
759
760
761
762
763
764
765
766
767
768
769
770
771
772
773
774
775
776
777
778
779
780
781
782
783
784
785
786
787
788
789
790
791
792
793
794
795
796
797
798
799
800
801
802
803
804
805
806
807
808
809
810
811
812
813
814
815
816
817
818
819
820
821
822
823
824
825
826
827
828
829
830
831
832
833
834
835
836
837
838
839
840
841
842
843
844
845
846
847
848
849
850
851
852
853
854
855
856
857
858
859
860
861
862
863
864
865
866
867
868
869
870
871
872
873
874
875
876
877
878
879
880
881
882
883
884
885
886
887
888
889
890
891
892
893
894
895
896
897
898
899
900
901
902
903
904
905
906
907
908
909
910
911
912
913
914
915
916
917
918
919
920
921
922
923
924
925
926
927
928
929
930
931
932
933
934
935
936
937
938
939
940
941
942
943
944
945
946
947
948
949
950
951
952
953
954
955
956
957
958
959
960
961
962
963
964
965
966
967
968
969
970
971
972
973
974
975
976
977
978
979
980
981
982
983
984
985
986
987
988
989
990
991
992
993
994
995
996
997
998
999
1000

Email: h.r.fuller@keele.ac.uk

Telephone: +44(0)1691 404693

Fax: +44(0)1691 404065

Abstract

Cardiac pathology is emerging as a prominent systemic feature of spinal muscular atrophy (SMA), but little is known about the underlying molecular pathways. Using quantitative proteomics analysis, we demonstrate widespread molecular defects in heart tissue from the Taiwanese mouse model of severe SMA. We identify increased levels of lamin A/C as a robust molecular phenotype in the heart of SMA mice, and show that lamin A/C dysregulation is also apparent in SMA patient fibroblast cells and other tissues from SMA mice. Lamin A/C expression was regulated in-vitro by knockdown of the E1 ubiquitination factor UBA1, a key downstream mediator of SMN-dependent disease pathways, converging on β -catenin signalling. Increased levels of lamin A are known to increase the rigidity of nuclei, inevitably disrupting contractile activity in cardiomyocytes. The increased lamin A/C levels in the hearts of SMA mice therefore provide a likely mechanism explaining morphological and functional cardiac defects, leading to blood pooling. Therapeutic strategies directed at lamin A/C may therefore offer a new approach to target cardiac pathology in SMA.

Introduction

Spinal muscular atrophy (SMA) is a debilitating genetic disorder, traditionally classified as a neuromuscular disease due to the characteristic pathology of lower motor neuron degeneration and progressive muscle wasting (1). Accumulating evidence of pathology outside of the neuromuscular system, however, suggests that SMA should now be considered as a systemic condition (2). SMA has an incidence of approximately 1 in 10,000 live births (3), and in ~95% of patients it is caused by homozygous loss of *SMN1* gene, resulting in insufficient levels of the ubiquitously expressed survival of motor neuron (SMN) protein (4). There is no cure for SMA, but the last few years have seen significant progress in the development of therapies aimed at alleviating symptoms by raising full-length SMN protein levels (5). Nusinersen (Spinraza™), an antisense oligonucleotide drug, is now widely available for children and young adults with SMA, and most recently, Zolgensma™ (previously known as AVXS-101), an adeno-associated virus-based gene replacement therapy, was given approval by the FDA for the treatment of SMA children under 2 years of age. Though undoubtedly an enormous step forward, none of the strategies that have been developed so far show complete efficiency (5–8). Coupled with uncertainties around long-term effectiveness and extremely high price of both strategies, there is keen interest to find alternative therapeutic strategies that could, in combination with SMN-targeted therapy, offer maximum therapeutic benefit to all SMA patients (9).

SMN perturbations influence organ development and function across multiple levels (2), and so it is likely that organ-specific and/or systemic therapy delivery may be necessary to fully rescue the SMA phenotype (5). For example, a systematic review of the literature in 2017 found 58 studies that reported on a total of 264 SMA patients with cardiac abnormalities (10). A common finding among the 77 patients with the most severe type of SMA (Type I) was

1
2
3 structural pathology, observed mainly in the septum and/or cardiac outflow tract. All of the
4
5 63 Type II SMA patients identified in the literature search had electrocardiogram (ECG)
6
7 abnormalities, while the 124 patients with Type III SMA had cardiac rhythm disorders and/or
8
9 structural abnormalities. In addition to the numerous reports of cardiac defects among SMA
10
11 patients, the systematic review identified 14 studies that have documented cardiac pathology
12
13 in mouse models of SMA (10). Common macroscopic findings include decreased heart size
14
15 and decreased thickness of the left ventricular wall and interventricular septum, while a
16
17 frequent microscopic observation was cardiac fibrosis, which was detected at a pre-
18
19 symptomatic stage of the disease in both severe and intermediate mouse models of SMA (10–
20
21 12). In addition, almost all studies of SMA mouse models reported bradyarrhythmias (10). A
22
23 more recent study of a severe mouse model of SMA at pre- and early symptomatic time
24
25 points confirmed many of these previous findings, but also noted significant pooling of blood
26
27 in the heart, together with disorganization of cardiomyocytes and lack of trabecular
28
29 compaction (13). These findings strongly resemble symptoms of cardiomyopathy (13), and
30
31 indicate serious consequences for the normal electrical and mechanical functioning of the
32
33 heart.
34
35
36
37
38
39
40
41

42 A recent gene-expression study of hearts from the “Taiwanese” mouse model of severe SMA
43
44 identified 205 genes that were down-regulated and 269 genes that were up-regulated at an
45
46 early symptomatic time-point (i.e. P5) (14). Several of these changes were tracked back to a
47
48 pre-symptomatic time-point, suggesting that cardiac defects might be attributable, at least in
49
50 part, to cell autonomous mechanisms (14). To the best of our knowledge, this is the first
51
52 study to date that has conducted a comprehensive analysis of molecular changes in the SMA
53
54 mouse heart, and whilst it has generated novel insights about changes to the transcriptome,
55
56 proteomic insights into the SMA heart are lacking. This is particularly important in the
57
58
59
60

1
2
3 context of emerging evidence showing that the SMN protein plays fundamental roles in
4 protein translation (15, 16). In this study, we have conducted a comprehensive quantitative
5 proteomics study of heart tissue from the Taiwanese mouse model of severe SMA and show
6 that there is widespread dysregulation of protein expression in SMA compared to controls.
7
8 We verified the robust increase of one of these proteins, lamin A/C, in the hearts of SMA
9 mice, and propose a role for lamin A/C in SMA cardiac pathology, strongly supported by
10 case reports of an adult form of SMA caused by mutations in the lamin A/C encoding gene,
11 *LMNA* (17, 18). As with a wide range of neuromuscular conditions caused by mutations in
12 *LMNA*, including Emery-Dreifuss muscular dystrophy, limb-girdle muscular dystrophy 1B,
13 and dilated cardiomyopathy, cardiac involvement was a notable feature in each case of
14 *LMNA*-associated SMA. A role for lamin A/C in SMA is strengthened further by experiments
15 in which we demonstrate dysregulation across other cells and tissues, and a mechanistic link
16 between lamin A/C and ubiquitin-like modifier activating enzyme 1 (UBA1) protein, a key
17 contributor to SMN-dependent disease pathways (19–21).
18
19
20
21
22
23
24
25
26
27
28
29
30
31
32
33
34
35
36
37
38
39

40 Results

41 42 43 44 **Quantitative proteomics analysis of heart tissue from severe SMA mice reveals** 45 **widespread molecular defects** 46 47

48
49 To determine the molecular consequences of SMN depletion in the heart of the Taiwanese
50 mouse model of severe SMA (22), a quantitative comparison of the SMA and age-matched
51 control heart proteome was undertaken using iTRAQTM mass spectrometry analysis. This
52 approach identified 3105 proteins in total (Supplementary Table 1), of which 2479 were
53 identified with a 5% local false-discovery rate. For reliable quantification, proteins identified
54
55
56
57
58
59
60

1
2
3 from just a single peptide were removed, after which, differentially expressed proteins were
4 identified by removal of proteins with a fold-change of less than 1.25, and finally, exclusion
5 of proteins with a p-value of >0.05 assigned to their fold changes. This left 383 proteins that
6 met the specified criteria for differential expression, of which 177 proteins were increased
7 and 206 were decreased in expression in SMA mouse heart compared to controls
8 (Supplementary Table 2). Twenty-one of the differentially expressed proteins were also
9 altered in expression at the gene level in a recent microarray study of hearts from SMA mice
10 at an early symptomatic time-point (i.e. P5) (14), of which 16 followed the same direction of
11 differential expression (Supplementary Table 3).
12
13
14
15
16
17
18
19
20
21
22
23
24
25

26 Gene ontology (GO) analysis using the DAVID platform (23, 24) highlighted enriched
27 biological processes and cellular components relating to the up- and down-regulated proteins,
28 respectively (Supplementary Table 4). A relatively high proportion of up-regulated proteins
29 were found to be blood-related ($n=16$), and although this compliments a previous report of
30 blood pooling in the hearts of the Taiwanese SMA mouse model (13), these proteins were
31 excluded from further analysis to retain focus on changes specific to the heart tissue. After
32 also removing keratin-associated proteins ($n=4$), the remaining proteins were then subject to
33 analysis using STRING 10 (25) to identify statistically significant associations between them.
34
35
36
37
38
39
40
41
42
43
44
45
46
47
48
49
50
51
52
53
54
55
56
57
58
59
60

Lamin A/C expression is dysregulated in severe SMA mice and SMA patient fibroblasts

One of the 383 differentially expressed proteins, lamin A/C, was of particular interest to us since mutations in *LMNA*, the lamin A/C encoding gene, are known to cause an adult form of SMA (17, 18). Additionally, the analysis of published proteomic studies of the neuromuscular system in SMA (26) identified lamin A/C as a conserved molecular change across three separate studies of SMA (27–29). To date, however, these findings do not appear to have been verified, nor has lamin A/C been studied in the context of SMN-dependent pathways in heart. We therefore chose to verify and understand the individual contributions of lamins A and C to the overall lamin A/C expression trend, using quantitative western blotting of heart tissue extracts from P8 SMA mice and healthy littermate controls (see workflow in Figure 2A). This analysis confirmed a robust increase in lamin A (69%, $p = 0.0007$) and C (91%, $p = 0.0079$) expression in SMA compared to control heart extracts (Figure 2B and 2C). Immunohistochemical analysis of SMA and control mouse heart sections revealed few lamin A/C positive cells in the ventricle lumen (Figure 2D), and although we cannot rule out a minor contribution, this result confirms that the increased lamin A/C levels cannot be solely attributed to circulating blood cells. Indeed, densitometry analysis of lamin A/C expression confirmed a robust upregulation of lamin A/C levels in the ventricle wall of SMA mouse heart sections compared to the unaffected controls (84%, $p = 0.0002$) (Figure 2E).

Protein extracts of SMA and control mouse brain, spinal cord, muscle, and liver tissue, as well as control and SMA patient dermal fibroblast extracts were analysed by quantitative western blotting to determine whether lamin A/C dysregulation extends beyond the heart. These analyses revealed widespread dysregulation of both lamin A and C, with differing

1
2
3 directions of expression change depending on the tissues examined (Figure 2B and 2C). A
4 statistically significant reduction of lamin A levels was seen in the SMA patient fibroblast
5 cells compared to those from healthy controls (84%, $p = 0.0438$), while a statistically
6 significant upregulation of lamin A levels was found in the brain (25%, $p = 0.0434$) and liver
7 (52%, $p = 0.0026$) tissue from SMA mice. Spinal cord extracts from SMA mice did not show
8 a significant change in lamin A expression compared to the healthy controls, but they did
9 show a significant increase in the levels of lamin C (43%, $p = 0.0078$), as did the liver (42%,
10 $p = 0.0075$) and brain (43%, $p = 0.0116$). Patient fibroblast cells, on the contrary, showed no
11 significant change in lamin C expression compared to the healthy controls, despite having a
12 drastic reduction in lamin A levels. It was not possible to reliably determine whether lamin A
13 or C were dysregulated in the skeletal muscle extracts due to large variability between
14 samples, for reasons we are unable to explain. Lamin A dysregulation in SMA patient
15 fibroblasts and SMA mouse heart (where protein levels were lowest, and highest, compared
16 to controls, respectively) appears to occur post-transcriptionally, since RT-qPCR analysis
17 showed no significant change in lamin A transcript levels in SMA compared to controls
18 (Figure 2F).

41 **Lamin A/C and UBA1 are mechanistically linked**

42 Having established the widespread dysregulation of lamin A/C levels across SMA patient
43 fibroblasts and mouse tissues (Figure 2), we next wanted to investigate whether there is a
44 relationship between lamin A/C and UBA1. The justification for this is that a role for UBA1
45 in SMN-dependent pathways has been well characterised across several models of SMA (19–
46 21), and previous research has shown that like UBA1 (19), lamin A/C is implicated in the
47 regulation of the β -catenin signalling pathway (30, 31). In addition, a previous study reported
48 decreased levels of UBA1 expression across a range of non-neuronal tissues from the
49
50
51
52
53
54
55
56
57
58
59
60

1
2
3 Taiwanese mouse model of SMA compared to controls, with the heart being most severely
4 affected, followed by the liver (20). This is of particular interest in context with the current
5 study, since heart tissue from SMA mice showed the greatest increase of lamin A/C levels
6 across the tissues examined, also followed by the liver (Figure 2). (SMA patient fibroblasts
7 appear to be an anomaly, as they were the only sample to show reduced lamin A levels
8 compared to controls but had unchanged levels of UBA1 (Supplementary File, S4)). To
9 investigate the relationship between lamin A/C, UBA1 and SMN, a western blot study of
10 their relative protein expression levels was conducted using equal amounts of total protein
11 from heart, muscle, liver, brain and spinal cord tissue extracts from healthy control mice and
12 from healthy human fibroblasts. This revealed a strong inverse pattern of lamin A/C and
13 UBA1 expression (Figure 3A) whereby the cells / tissues typically considered under the most
14 mechanical strain (i.e. fibroblast cells, heart and muscle tissue) had high relative levels of
15 lamin A/C and low relative levels of UBA1. Tissues under the least mechanical strain (i.e.
16 liver, brain and spinal cord) showed the opposite pattern, with low relative levels of lamin
17 A/C and high relative levels of UBA1 (Figure 3A). SMN followed the same expression trend
18 as UBA1 across the tissues examined (Figure 3A).

19
20
21
22
23
24
25
26
27
28
29
30
31
32
33
34
35
36
37
38
39
40
41
42 Having established an inverse correlation between UBA1 and lamin A/C expression across a
43 range of tissues, we next wanted to determine whether a mechanistic link exists between
44 them. Knockdown of UBA1 expression in human embryonic kidney (HEK) cells resulted in a
45 ~43% upregulation of lamin A expression ($p = 0.0398$), independent of changes to lamin C
46 and SMN (Figure 3B). We also examined mouse embryonic fibroblast cells lacking the
47 *LMNA* gene (32), and found that UBA1 (55%, $p = 0.0053$) and SMN (21%, $p = 0.0016$) were
48 significantly reduced compared to the control (Figure 3C). Immunostaining of control and
49 SMA patient fibroblasts showed colocalisation between UBA1 and lamin A at the nuclear
50
51
52
53
54
55
56
57
58
59
60

1
2
3 periphery in control and SMA cells (Figure 4A), indicating a possible interaction between
4
5 lamin A/C and UBA1. To investigate this further, an immunoprecipitation from control and
6
7 SMA mouse heart extracts was performed using a lamin A/C monoclonal antibody attached
8
9 to magnetic beads. Although both lamin A/C and UBA1 were easily detected in SMA and
10
11 control heart extracts by western blot analysis, UBA1 was undetectable in the eluates
12
13 following pull-down (Figure 4B). It is important to note though that an interaction between
14
15 lamin A/C and UBA1 cannot be ruled out on this basis since physiological interactions may
16
17 occur between a minor proportion of the total protein present and/or it may be vulnerable to
18
19 disruption by protein extraction methods (33). Interestingly, however, we did find that a small
20
21 proportion of the total β -catenin co-immunoprecipitated with lamin A/C from both SMA and
22
23 control heart extracts, providing evidence that lamin A/C interacts with β -catenin in the heart
24
25 under normal physiological conditions (Figure 4B). When taken together, these experiments
26
27 demonstrate a mechanistic link between lamin A/C and UBA1, a proven contributor to SMN-
28
29 dependent disease pathways, and highlight β -catenin signalling as a potential pathway upon
30
31 which they both converge.
32
33
34
35
36
37
38
39
40
41

42 **Discussion**

43
44 A small percentage of SMA cases are associated with mutations in genes other than *SMN*,
45
46 including *UBA1* (34), *GARS1* (35) and *LMNA* (17, 18). Mutations in the *UBA1* gene, which
47
48 encodes the UBA1 protein, cause a form of X-linked infantile SMA (SMAX2) (34), and a
49
50 role for UBA1 in SMN-dependent pathways has also been well characterised across several
51
52 models of SMA (19–21). Mutations in *GARS1* are known to cause infantile (36, 37) as well
53
54 as an adult onset type of SMA (35). Dysregulation of UBA1/GARS1 pathways disrupted
55
56 sensory neuron fate and altered sensory-motor connectivity in SMA mice, both of which were
57
58
59
60

1
2
3 corrected following restoration of UBA1 levels (21). Unlike *UBA1* and *GARS1*, however, the
4 involvement of *LMNA* in SMN-dependent disease pathways has so far been unexplored.
5
6 Here, we demonstrated that there are widespread molecular defects in heart tissue from the
7
8 Taiwanese mouse model of severe SMA, one of which is the protein product of the *LMNA*
9
10 gene, lamin A/C. We verified the robust increase of lamin A/C in the hearts from SMA mice,
11
12 and have identified a mechanistic link between UBA1 and lamin A/C.
13
14
15
16
17
18

19 The A-type lamins, lamin A and C, are encoded by *LMNA* gene, and in addition to providing
20 structural support to the nucleus, are involved in several other functions including
21 mechanosignaling, chromatin organization and regulation of gene expression (38). Mutations
22 in *LMNA* gene cause a spectrum of disorders known as laminopathies, the majority of which
23 prominently feature cardiac pathology. The adult form of SMA caused by *LMNA* mutations is
24 no exception to this, as each of the patients described experienced cardiac problems with
25 disease progression and required a pacemaker. Examination of family history in each case
26 also revealed a high frequency of cardiac abnormalities and sudden unexplained cardiac
27 deaths (15, 16). This indisputable link between lamin A/C mutations and cardiac pathology in
28 a wide range of conditions, including a rare form of SMA, leaves very little doubt that correct
29 functioning of lamin A/C is a key requirement for the maintenance of cardiac health. The
30 finding here that lamin A/C is robustly increased in heart tissue from a mouse model of SMA
31 therefore strongly suggests that lamin A/C is responsible, at least in part, for previously
32 reported cardiac defects in SMA.
33
34
35
36
37
38
39
40
41
42
43
44
45
46
47
48
49
50
51
52
53

54 Lamin A/C plays a significant role in the regulation of cell stability and cell dynamics (39),
55 and its expression levels correlate with tissue stiffness, where rigid tissues have the highest
56 levels and softer tissues the least (40). This therefore suggests that changes in lamin A/C
57
58
59
60

1
2
3 expression may be most pathologically relevant in SMA in highly mechanically active tissues
4 such as the heart, where increased expression of lamin A/C is likely to impair its proper
5
6 functioning. Indeed, increased rigidity of human and rat cardiomyocytes increased the extent
7
8 to which cells/tissues resist deformation (i.e. passive tension) *in-vitro* (41, 42), and *in-vivo* rat
9
10 experiments showed that higher passive tension slows the dynamics of myocardium
11
12 contractions and induces functional heart defects (42). Increased cardiomyocyte rigidity was
13
14 also identified in a cell model carrying a mutation in the *LMNA* gene (43). This mutation
15
16 causes severe dilated cardiomyopathy in humans (43), which strongly mirrors the phenotype
17
18 previously observed in severe and mild mouse models of SMA, including thinning of
19
20 ventricle walls and interventricular septum (11, 13), and dilation of ventricles (13, 44, 45).
21
22 The pathological end-point of dilated cardiomyopathy is systolic heart failure where the heart
23
24 cannot pump blood properly. This would be evidenced by decreased ejection fraction and
25
26 blood pooling in ventricles; both of which were identified in SMA mice (13, 44–46) and
27
28 SMA patients (18, 47, 48). In the context of SMN-dependent SMA, it seems highly likely,
29
30 therefore, that increased levels of lamin A/C would lead to stiffening of the cardiomyocytes,
31
32 impeding their ability to contract properly and inducing the cardiac defects previously
33
34 reported in SMA. In addition, cardiac fibrosis has been described in patients harbouring a
35
36 *LMNA* mutation (49, 50), and was frequently reported in SMA patients and mouse models of
37
38 SMA (10), even at a pre-symptomatic stage of the disease in both severe and intermediate
39
40 mouse models of SMA (11, 12). As cardiac fibrosis is a key regulator of myocardial rigidity
41
42 (42), it is therefore possible that this might further exacerbate problems described above
43
44 (Figure 5).
45
46
47
48
49
50
51
52
53
54
55

56 A role for lamin A/C in SMA is strengthened further by our data demonstrating a mechanistic
57
58 link between lamin A/C and UBA1, a key contributor to SMN-dependent disease pathways
59
60

1
2
3 (19–21). It seems highly likely that this mechanism converges on the β -catenin signalling
4 pathway, since both lamin A/C and UBA1 are implicated in its regulation (19, 30, 31). UBA1
5 controls the stability of β -catenin through the canonical ubiquitin-proteasome pathway, and
6 deficiency in UBA1 protein levels leads to β -catenin accumulation and neuromuscular
7 pathology in SMA (19). Defective Wnt/ β -catenin signalling was found to contribute to the
8 pathology of dilated cardiomyopathy caused by mutation in *LMNA* gene (30), and in a
9 separate study, lamin A/C was shown to regulate the differentiation fate of mesenchymal
10 stem cells (MSCs) by controlling dynamics of the Wnt/ β -catenin signalling pathway (31).
11 Lamin A/C overexpression, for example, increased nuclear levels of β -catenin and activated
12 the Wnt signalling pathway to promote osteoblast differentiation (31). The same study also
13 provided evidence of an interaction between lamin A/C and β -catenin by
14 immunoprecipitation of nuclear proteins from MSCs forcibly overexpressing lamin A/C (31).
15 This physical interaction was proposed as a mechanism by which β -catenin is translocated to
16 the nucleus (31). Here, we further expanded the knowledge of the relationship between lamin
17 A/C and β -catenin, by demonstrating an interaction between them in heart extracts under
18 normal physiological conditions.
19
20
21
22
23
24
25
26
27
28
29
30
31
32
33
34
35
36
37
38
39
40
41

42 The arguments above support the hypothesis that lamin A/C dysregulation is likely to be
43 responsible, at least in part, for previously reported cardiac defects in SMA, but other
44 proteins identified in this screen also offer insight into the molecular defects underlying
45 cardiac abnormalities in SMA. For example, two such proteins, SUN domain-containing
46 protein 2 (SUN2) (51) and cell division cycle 5-like protein (Cdc5l) (52), are known lamin
47 A/C interactors and may provide further insights into lamin A/C-associated pathways in
48 SMA. Like *LMNA*, mutations in *SUN2*, the gene encoding the SUN2 protein, have been
49 associated with Emery-Dreifuss muscular dystrophy, a neuromuscular disorder often
50
51
52
53
54
55
56
57
58
59
60

1
2
3 associated with cardiac defects (53). Cdc5l, on the other hand, is a known splicing complex
4 component that appears to require lamin A/C in order to regulate its assembly and targeting
5 to the spliceosomal complex (52). Alterations to this interaction may therefore affect splicing
6 and gene transcription, further exacerbating the downstream molecular consequences of
7 reduced SMN expression. With this in mind, it is interesting to note that a large proportion of
8 the down-regulated proteins in the SMA mouse heart were associated with translation, and re-
9 enforces previous work showing that the SMN protein plays fundamental roles in protein
10 translation (15, 16). It is also highly relevant that we found a large proportion of the down-
11 regulated proteins in the SMA heart to be associated with metabolic processes, while the up-
12 regulated proteins were strongly associated with cytoskeletal and extracellular matrix
13 organisation (Figure 1). Imbalances in contractile performance are known to promote
14 remodelling and dedifferentiation of adult cardiomyocytes; the consequences of which
15 include cytoskeletal rearrangement, restructuring of contractile apparatus, and reduced
16 oxidative metabolism (54). Ironically, it seems that these adaptive processes - presumably
17 intended to protect the cardiomyocytes in times of mechanical and/or molecular stress – can
18 lead to adverse consequences for the heart (54). Disruption of actin cytoskeleton, for
19 example, can impair contractile properties of cardiomyocytes and was implicated in initiation
20 of cardiomyocyte apoptosis (55).
21
22
23
24
25
26
27
28
29
30
31
32
33
34
35
36
37
38
39
40
41
42
43
44
45
46

47 Here we have offered new insight into the molecular defects underlying cardiac abnormalities
48 in SMA, but other important questions remain that are worthy of further attention. It would
49 be of interest in the future, for example, to explore the functional consequences of lamin A/C
50 dysregulation in other cells and tissues throughout the natural history of disease progression
51 in SMA. Moreover, identification of upstream regulators of lamin A/C may help to unravel
52 the tissue-specific regulatory mechanisms that act on lamin A/C in response to SMN
53
54
55
56
57
58
59
60

1
2
3 depletion. Finally, and most importantly, it will be crucial to determine the extent to which
4
5 SMN-replacement therapies reverse the molecular defects in SMA, and whether this is
6
7 sufficient to fully rescue the cardiac defects widely reported across SMA patients and mouse
8
9 models. When doing so, it would be important to monitor cardiac health longitudinally to
10
11 determine whether new phenotypes emerge following long-term SMN-replacement therapy,
12
13 and with increasing age. Therapies primarily designed to target neuronal tissues, such as
14
15 Nusinersen, are especially relevant in this context since they are unlikely to rescue
16
17 pathological defects in SMA heart. This knowledge, together with a broader understanding of
18
19 the interplay between lamin A/C and other regulators of heart function in SMA, would help
20
21 to isolate the most appropriate targets for therapy design that could, in combination with
22
23 SMN-targeted therapy, offer maximum therapeutic benefit to all SMA patients.
24
25
26
27
28
29
30
31
32

33 **Materials and Methods**

34 35 36 37 **Spinal muscular atrophy mouse model**

38
39 The Taiwanese mouse model (original strain purchased from Jackson Laboratories, No.
40
41 005058), heterozygous for the SMN2 transgene on *Smn* null background (*Smn*^{-/-}; *SMN2*^{tg/+})
42
43 (22) and age-matched phenotypically normal controls (*Smn*^{+/-}; *SMN2*^{tg/o}) were maintained in
44
45 SPF facilities at the University of Edinburgh. The breeding strategy, and genotyping using
46
47 standard PCR protocols, were employed as previously described (56). Tissue was harvested
48
49 at a symptomatic time point, postnatal day 8 (P8). All animal work was carried under the
50
51 appropriate Project and Personal Licenses from the UK Home Office (PPL:60/4569) and
52
53 following local ethical review.
54
55
56
57
58
59
60

Quantitative proteomics analysis

Total protein extracts were prepared from the hearts of postnatal day 8 (P8) SMA mice (n = 5) and healthy littermate mice (n = 5) for iTRAQ quantitative mass spectrometry analysis as previously described (57). Following trypsin digestion, peptides were labelled with iTRAQ™ tagging reagents according to the protocol in the iTRAQ kit and were assigned to each sample group as follows: 114-control and 115-SMA.

High pH reverse-phase liquid chromatography (RPLC) fractionation

All iTRAQ labelled peptides were combined into one tube, concentrated using a vacuum concentrator (ThermoSavant, ThermoFisher Scientific) and resuspended in 100 µl of buffer A (10 mM ammonium formate (NH₄HCO₂), 2 % acetonitrile (MeCN), pH 10.0). The peptides were then fractionated by high pH reverse-phase liquid chromatography (RPLC) using a C18 column (XBridge C18 5 µm, 4.6 x 100 mm, Waters). The column was rinsed with 96 % buffer A at 1 mL/min for 6 minutes until the optical density (OD) on the ultraviolet chromatogram returned to the baseline. The gradient ran from 4-28 % of buffer B (10 mM NH₄HCO₂, 90 % MeCN, pH 10.0) for 30 minutes to 28-50 % buffer B for 6 minutes. The column was rinsed in 80 % buffer B for 5 minutes and then was re-equilibrated at initial conditions with 4 % buffer B for 11 minutes. Fractions of 0.5 mL were collected every 30 seconds. The UV chromatogram was analysed and the fractions with similar peptide concentration across the elution profile were combined to give 12 fractions. The pooled fractions were concentrated in a vacuum concentrator and resuspended in 30 µl of 0.1 % formic acid (FA).

Liquid chromatography-tandem mass spectrometry (LC-ESI-MS/MS) analysis

1
2
3 One third of each fraction containing the labelled peptides was analysed by mass
4 spectrometry. Peptides were separated by liquid chromatography (LC) using a nanoLC Ultra
5 2D plus loading pump and nanoLC AS-2 autosampler chromatography system (Eksigent).
6
7 Peptides were loaded with buffer A (2% MeCN, 0.05% TFA in ultrapure water) and bound to
8 an Acclaim PepMap100 trap (100 μm x 2 cm) (ThermoFisher Scientific). The trap was then
9 washed for 10 minutes with buffer A, after which the trap was turned in-line with the
10 analytical column (Acclaim PepMap RSLC column, 75 μm x 15 cm). The analytical solvent
11 system consisted of buffer A and buffer B (98 % MeCN, 0.1 % FA in ultrapure water) at 300
12 nl/min flow rate. Peptides were eluted using the followed gradient: linear 2-20 % of buffer B
13 over 90 minutes, linear 20-40 % of buffer B for 30 minutes, linear 40-98% of buffer B for 10
14 minutes, isocratic 98% of buffer B for 5 minutes, linear 98-2% of buffer B for 2.5 minutes
15 and isocratic 2% buffer B for 12.5 minutes. The eluent was sprayed with a NANOSpray II
16 source (electrospray ionization, ESI) into the TripleTOF 5600+ tandem mass spectrometer
17 (AB Sciex), controlled by Analyst® TF software (AB Sciex). The mass spectrometer was
18 operated in data-dependent acquisition (DDA) top20 positive ion mode with 120 ms
19 acquisition time for MS (m/z 400-1250) and 80ms for MS/MS (m/z 95-1800), and 15 seconds
20 of dynamic exclusion. MS/MS was conducted with a rolling collision energy (CE) inclusive
21 of present iTRAQ CE adjustments.
22
23
24
25
26
27
28
29
30
31
32
33
34
35
36
37
38
39
40
41
42
43
44
45
46

47 The twelve raw mass spectrometry data files were analysed by ProteinPilot software, version
48 5.0.1.0 (Applied Biosystems) with the Paragon™ database search and Pro Group™
49 Algorithm using the UniProtKB/Swiss-Prot FASTA database. The general Paragon search
50 analysis parameters were: type 'iTRAQ4plex (Peptide Labeled)', cysteine alkylation
51 'MMTS', digestion 'trypsin' as the cleavage enzyme, instrument 'TripleTOF, and species
52 'Mouse' for sample parameters; processing parameters were specified as 'quantitative', 'bias
53
54
55
56
57
58
59
60

1
2
3 correction', 'background correction'; 'thorough ID' and 'biological modifications'. Proteins
4
5 that showed a Protein Threshold > 5 were used for the Pro Group Algorithm to calculate the
6
7 relative quantification of the protein expression, generating an error factor and p-value. A
8
9 false discovery rate (FDR) analysis was performed using the Proteomics System Performance
10
11 Evaluation Pipeline (PSPEP).
12
13
14
15
16

17 **Bioinformatics analysis**

18
19 The Database for Annotation, Visualization and Integrated Discovery (DAVID 6.8) (23, 24)
20
21 was used for the gene ontology (GO) analysis. The analysis was performed separately for
22
23 upregulated and downregulated proteins, and included terms with at least two annotated
24
25 proteins and p-value ≤ 0.05 . Differentially expressed proteins were also analysed using the
26
27 Search Tool for the Retrieval of Interacting Genes/Proteins (STRING) 10 (25) to identify
28
29 statistically significant interactions between them. Association network analysis was
30
31 performed with high confidence (0.700) interaction score for upregulated and with highest
32
33 confidence (0.900) interaction score for downregulated proteins to exclude false positive
34
35 results.
36
37
38
39
40
41
42

43 **Cell culture**

44
45 Skin fibroblast cells from the Coriell Cell Repository (Supplementary File, S1) were grown in
46
47 high glucose Dulbecco's Modified Eagle Medium (DMEM; Gibco) with 10% fetal bovine
48
49 serum (FBS; Gibco) supplemented with 1% non-essential amino acids (MEM-NEAA; Gibco)
50
51 and 1 % penicillin-streptomycin (PEN-STREP; Lonza). Wild type and *LMNA* knockout
52
53 mouse embryonic fibroblast cells (MEFs) (32) were grown in DMEM (Gibco) with 15% FBS
54
55 (Gibco) supplemented with 1% MEM-NEAA (Gibco) and 1 % PEN-STREP (Lonza).
56
57
58
59
60

1
2
3 HEK293 cells were obtained from European Collection of Authenticated Cell Cultures. Cell
4 culture and knockdown of ubiquitin-like modifier-activating enzyme 1 (UBA1) was
5 performed as previously described (21). Briefly, HEK293 cells were grown in DMEM (Life
6 Technologies) with 10% FBS (Sigma), penicillin/streptavidin (Invitrogen) and L-glutamine
7 (Invitrogen). Cells were transfected with RNAiMax (Invitrogen) and 2.5 μ M Silencer Select
8 Validated *UBA1* siRNA (s601, targeted against exons 24 and 25; Life Technologies) or
9 2.5 μ M negative control siRNA 2 (Life Technologies) according to the manufacturer's
10 instructions. Control (CTR) and UBA1 knockdown (UBA1 KD) HEK cells were harvested
11 48h after transfection.
12
13
14
15
16
17
18
19
20
21
22
23
24
25

26 **Western blotting**

27
28 Protein extraction, SDS-PAGE and western blotting were performed as previously described
29 (58). Briefly, after SDS-PAGE a part of the gel was excised and stained with Coomassie blue
30 as an internal loading control for total protein. Proteins from the remaining part of the gel
31 were transferred to nitrocellulose membrane by western blotting overnight. Membranes were
32 blocked with 4% powdered milk and incubated with primary antibodies in dilution buffer
33 (1% FBS, 1% horse serum, 0.1% BSA in PBS with 0.05% Triton X-100) for a maximum of
34 two hours. Primary antibodies were as follows: mouse anti-SMN (MANSMA12 2E6 (59);
35 1:100), rabbit anti-UBA1 (Novus; NBP2-67816; 1:500-1:1000), mouse anti-lamin AC
36 (MANLAC1 4A7 (60); 1:100) was used for cell extracts and rabbit anti-lamin AC (Abcam;
37 ab169532; 1:2000) was used for tissue extracts. Following incubation with HRP-labelled
38 rabbit anti-mouse Ig (DAKO, P0260) or HRP-labelled goat anti-rabbit Ig (DAKO, P0488) in
39 dilution buffer at 0.25 ng/mL, membranes were incubated with West Pico or West Femto
40 (Thermo Fisher) and visualised using a Gel Image Documentation system (Biorad).
41
42
43
44
45
46
47
48
49
50
51
52
53
54
55
56
57
58
59
60 Densitometry measurements of antibody reactive bands were obtained using Fiji software

(v1.51) (61) and were normalised to densitometry measurements of the Coomassie stained gel. For densitometry measurements only, contrast and brightness were adjusted uniformly across the gel and blot to decrease the background and enhance signal detection.

RT-qPCR

Total RNA was extracted using RNeasy Plus Mini kit (Qiagen) and quantified with a NanoDrop ND- 1000 spectrophotometer (Thermo Fisher). Absorption ratios (OD_{260}/OD_{280} nm; OD_{260}/OD_{230} nm) were used to verify the integrity of the RNA. Total RNA was reverse transcribed using SuperScrip VILO cDNA Synthesis Kit (Invitrogen). Quantitative PCR was performed in QuantStudio 3 Real Time PCR system (Applied Biosystems), using SYBR Green detection system (SYBR Select Master Mix; Applied Biosystems). All PCR reactions were performed in triplicates and contained 3.75 ng of cDNA (fibroblast cells) or 2.8 ng of cDNA (heart tissue), and 300 nM Forward and 300 nM Reverse primers in the final volume of 20 μ L. Parallel wells with no cDNA (NTC; no-template controls) were run for each gene to control for contamination. RNA Polymerase II Subunit J (*POLR2J*) and TATA-Box binding protein (*TBP*) were used as reference genes as they have previously demonstrated stable expression across tissues (62). Relative gene expression was quantified using Pfaffl method (63). The parameters of the reactions were 50°C for 2 min, 95°C for 10 min, and 40 cycles of 95°C for 15 sec and 60°C for 1 min. Dissociation curves were obtained for each sample and PCR products were run on 1% agarose gel for a quality control. Primer sequences for lamin A, *POLR2J* and *TBP* are available in the Supplementary File (S2). Efficiency of the primer pairs was determined by making serial dilutions of the cDNA, plotting the log values of the cDNA against the C_t (cycle threshold) values, and using a slope to calculate the efficiency according to the equation: $E = 10^{[-1/\text{slope}]} \times 100$ (63).

Immunohistochemistry (IHC)

SMA and control mouse hearts were fixed in 4% paraformaldehyde for 4 hours, cryopreserved in 30% sucrose solution with 0.1% sodium azide and subsequently embedded in a 1:1 solution of 30% sucrose and optimum cutting temperature compound (OCT) at -40°C. Ventricular heart sections (7µm) were air dried for 1 hour and subjected to antigen retrieval by submersion for 20 minutes in 10mM sodium citrate buffer at 90°C, followed by 30 minutes cooling remaining in solution. Sections were incubated for 2 hours in blocking solution (0.4% bovine serum albumin (BSA), 1% Triton X-100 in 0.1M PBS) at 4°C and then overnight with rabbit anti-lamin A/C antibody (Novus; NBP2-19324) at 4°C. Slides were washed twice (10 minutes each in PBT (0.1M phosphate buffered saline (PBS) with 0.1% Tween-20)), followed by one 10 minute wash in 0.1M PBS. Sections were incubated with Cy3 goat anti-rabbit IgG (H+L) (ThermoFisher; A10520) for 2 hours at 4°C, with successive washes as before. Sections were mounted using MOWIOL media (10% Mowiol (Sigma; 81381), 20% glycerol, 50% 0.2M Tris buffer pH 8.5, 3% 1,4-diazobicyclooctance made up in distilled water) containing 4',6-diamidino-2-phenylindole (DAPI).

For the Figure, sections were imaged using Nikon eclipse e400 microscope (20x objective). For the purpose of quantification, sections were imaged using a Zeiss LSM710 inverted confocal microscope (63x objective). Densitometry measurements of lamin A/C staining in the heart ventricles were performed using Fiji software (version 1.51) (61). Images were calibrated to optical density (OD) as previously described (58), and rectangular selection tool of fixed size was used to measure OD of the ventricle wall. Prior to statistical analysis, the OD of the background was subtracted from the OD measurements of the ventricle wall. Nine sections from each mouse were used in the analysis.

Immunocytochemistry

Fibroblast cells were fixed in acetone: methanol solution (50:50) for 10 minutes, washed with PBS three times for five minutes and incubated with rabbit anti-UBA1 (Novus; NBP2-67816; 1:100) and mouse anti-lamin A (Santa Cruz; sc-71481; 1:50) in blocking buffer (1% FBS and 1% HS in PBS) for one or two hours. After incubation with goat anti-rabbit IgG Alexa Fluor 488 and anti-mouse IgG Alexa Fluor 546 (Life Technologies; 5 µg/mL) in blocking buffer for one hour, cells were stained with DAPI (Sigma; 0.4 µg/mL) for 10 minutes and mounted using Hydromount (National diagnostics). Between each step cells were washed with PBS three times for five minutes. Images were obtained using Leica SP5 confocal microscope with 63× oil immersion objective.

Immunoprecipitation

Immunoprecipitation was performed as described previously (64). Briefly, anti-mouse Pan Ig-coated magnetic beads (50µl) (Dyna, Oslo) were washed with 4% BSA in PBS, then incubated with an anti-lamin A/C monoclonal antibody (26) (neat, 50µl) for 1 hour at room temperature with gentle rolling. The beads were then washed and incubated for 1 hour at room temperature with RIPA extracts of heart tissue from SMA and healthy littermate control mice (15µl) on a roller. The beads were washed thoroughly with RIPA buffer before eluting captured material by heating at 90°C for 3 minutes in 1 x SDS sample buffer (30µl) (2% sodium dodecyl sulphate- SDS, 10% glycerol, 5% 2-mercaptoethanol, 62.5 mM Tris-HCl, pH 6.8). Samples were subjected to western blotting as described above. Primary antibodies were as follows: rabbit anti-lamin AC (Abcam; ab169532; 1:2000), rabbit anti-UBA1 (Novus; NBP2-67816; 1:1000) and mouse anti-β-catenin (BD Transduction Laboratories; 610154; 1:1000).

Statistical analysis

All statistical analyses were performed in GraphPad Prism version 8.0.1 for Windows, GraphPad Software, San Diego, California USA, www.graphpad.com. The Shapiro-Wilk test was first used to assess the distribution of the data, followed by unpaired two-tailed *t*-test for parametric data, and a Mann-Whitney *U* test for a non-parametric data. All data are presented as mean +SD. Statistical significance was considered to be $p \leq 0.05$ for all analyses.

Supplementary material

Supplementary Material is available at...

Acknowledgements

The authors would like to thank Prof Colin L Stewart, Institute of Medical Biology, Singapore, for kindly providing wild type and *LMNA* knockout mouse embryonic fibroblasts, and Prof Glenn E Morris for helpful discussions about lamin A and for providing access to laboratory equipment. This research was supported by funding from the Newlife Charity [SG/15-16/11] (HF) and Keele University ACORN funding (HF & DS); British Heart Foundation [PG/16/68/31991] (IH); UK SMA Research Consortium (SMA Trust) (THG) and the Euan MacDonald Centre for Motor Neurone Disease Research (HKS and THG); and Wellcome Trust [094476/Z/10/Z] (SLS).

Conflict of interest statement

THG is a member of SMA-related advisory boards for Roche, Muscular Dystrophy UK and SMA Europe.

References

1. Groen, E.J.N., Talbot, K. and Gillingwater, T.H. (2018) Advances in therapy for spinal muscular atrophy: promises and challenges. *Nat. Rev. Neurol.*, **14**, 214–224.
2. Simone, C., Ramirez, A., Bucchia, M., Rinchetti, P., Rideout, H., Papadimitriou, D., Re, D.B. and Corti, S. (2016) Is Spinal Muscular Atrophy a disease of the motor neurons only: pathogenesis and therapeutic implications? *Cell. Mol. Life Sci.*, **73**, 1003–1020.
3. Verhaart, I.E.C., Robertson, A., Wilson, I.J., Aartsma-Rus, A., Cameron, S., Jones, C.C., Cook, S.F. and Lochmüller, H. (2017) Prevalence, incidence and carrier frequency of 5q-linked spinal muscular atrophy—a literature review. *Orphanet J. Rare Dis.*, **12**.
4. Lefebvre, S., Burglen, L., Reboullet, S., Clermont, O., Burlet, P., Viollet, L., Benichou, B., Cruaud, C., Millasseau, P., Zeviani, M., *et al.* (1995) Identification and characterization of a spinal muscular atrophy-determining gene. *Cell*, **80**, 155–165.
5. Sumner, C.J. and Crawford, T.O. (2018) Two breakthrough gene-targeted treatments for spinal muscular atrophy: challenges remain. *J. Clin. Invest.*, **128**, 3219–3227.
6. Finkel, R.S., Mercuri, E., Darras, B.T., Connolly, A.M., Kuntz, N.L., Kirschner, J., Chiriboga, C.A., Saito, K., Servais, L., Tizzano, E., *et al.* (2017) Nusinersen versus Sham Control in Infantile-Onset Spinal Muscular Atrophy. *N. Engl. J. Med.*, **377**, 1723–1732.
7. Mercuri, E., Darras, B.T., Chiriboga, C.A., Day, J.W., Campbell, C., Connolly, A.M., Iannaccone, S.T., Kirschner, J., Kuntz, N.L., Saito, K., *et al.* (2018) Nusinersen versus Sham Control in Later-Onset Spinal Muscular Atrophy. *N. Engl. J. Med.*, **378**, 625–635.
8. Mendell, J.R., Al-Zaidy, S., Shell, R., Arnold, W.D., Rodino-Klapac, L.R., Prior, T.W., Lowes, L., Alfano, L., Berry, K., Church, K., *et al.* (2017) Single-Dose Gene-Replacement Therapy for Spinal Muscular Atrophy. *N. Engl. J. Med.*, **377**, 1713–1722.
9. Bowerman, M. (2019) Funding for spinal muscular atrophy research must continue. *Futur.*

- 1
2
3 *Neurol*, **14**.
4
5
6 10. Wijngaarde, C.A., Blank, A.C., Stam, M., Wadman, R.I., Van Den Berg, L.H. and Van
7
8 Der Pol, W.L. (2017) Cardiac pathology in spinal muscular atrophy: a systematic
9
10 review. *Orphanet J. Rare Dis.*, **12**.
11
12 11. Shababi, M., Habibi, J., Yang, H.T., Vale, S.M., Sewell, W.A. and Lorson, C.L. (2010)
13
14 Cardiac defects contribute to the pathology of spinal muscular atrophy models. *Hum.*
15
16 *Mol. Genet.*, **19**, 4059–4071.
17
18 12. Cobb, M.S., Rose, F.F., Rindt, H., Glascock, J.J., Shababi, M., Miller, M.R., Osman,
19
20 E.Y., Yen, P.-F., Garcia, M.L., Martin, B.R., *et al.* (2013) Development and
21
22 characterization of an SMN2-based intermediate mouse model of Spinal Muscular
23
24 Atrophy. *Hum. Mol. Genet.*, **22**, 1843–1855.
25
26 13. Maxwell, G.K., Szunyogova, E., Shorrock, H.K., Gillingwater, T.H. and Parson, S.H.
27
28 (2018) Developmental and degenerative cardiac defects in the Taiwanese mouse model
29
30 of severe spinal muscular atrophy. *J. Anat.*, **232**, 965–978.
31
32 14. Sheng, L., Wan, B., Feng, P., Sun, J., Rigo, F., Bennett, C.F., Akerman, M., Krainer, A.R.
33
34 and Hua, Y. (2018) Downregulation of Survivin contributes to cell-cycle arrest during
35
36 postnatal cardiac development in a severe spinal muscular atrophy mouse model. *Hum.*
37
38 *Mol. Genet.*, **27**, 486–498.
39
40 15. Sanchez, G., Dury, A.Y., Murray, L.M., Biondi, O., Tadesse, H., El Fatimy, R., Kothary,
41
42 R., Charbonnier, F., Khandjian, E.W. and Côté, J. (2013) A novel function for the
43
44 survival motoneuron protein as a translational regulator. *Hum. Mol. Genet.*, **22**, 668–
45
46 684.
47
48 16. Bernabò, P., Tebaldi, T., Groen, E.J.N., Quattrone, A., Gillingwater, T.H. and Viero, G.
49
50 (2017) In Vivo Translatome Profiling in Spinal Muscular Atrophy Reveals a Role for
51
52 SMN Protein in Ribosome Biology. *Cell Rep.*, **21**, 953–965.
53
54
55
56
57
58
59
60

- 1
2
3 17. Rudnik-Schöneborn, S., Botzenhart, E., Eggermann, T., Senderek, J., Schoser, B.G.H.,
4
5 Schröder, R., Wehnert, M., Wirth, B. and Zerres, K. (2007) Mutations of the LMNA
6
7 gene can mimic autosomal dominant proximal spinal muscular atrophy. *Neurogenetics*,
8
9 **8**, 137–142.
10
11
- 12 18. Iwahara, N., Hisahara, S., Hayashi, T., Kawamata, J. and Shimohama, S. (2015) A novel
13
14 lamin A/C gene mutation causing spinal muscular atrophy phenotype with cardiac
15
16 involvement: report of one case. *BMC Neurol.*, **15**, 269.
17
18
- 19 19. Wishart, T.M., Mutsaers, C.A., Riessland, M., Reimer, M.M., Hunter, G., Hannam, M.L.,
20
21 Eaton, S.L., Fuller, H.R., Roche, S.L., Somers, E., *et al.* (2014) Dysregulation of
22
23 ubiquitin homeostasis and β -catenin signaling promote spinal muscular atrophy. *J. Clin.*
24
25 *Invest.*, **124**, 1821–1834.
26
27
- 28 20. Powis, R.A., Karyka, E., Boyd, P., Côme, J., Jones, R.A., Zheng, Y., Szunyogova, E.,
29
30 Groen, E.J.N., Hunter, G., Thomson, D., *et al.* (2016) Systemic restoration of UBA1
31
32 ameliorates disease in spinal muscular atrophy. *JCI Insight*, **1**, e87908.
33
34
- 35 21. Shorrock, H.K., Van Der Hoorn, D., Boyd, P.J., Llaverro Hurtado, M., Lamont, D.J.,
36
37 Wirth, B., Sleight, J.N., Schiavo, G., Wishart, T.M., Groen, E.J.N., *et al.* (2018)
38
39 UBA1/GARS-dependent pathways drive sensory-motor connectivity defects in spinal
40
41 muscular atrophy. *Brain*, **141**, 2878–2894.
42
43
- 44 22. Hsieh-Li, H.M., Chang, J.-G., Jong, Y.-J., Wu, M.-H., Wang, N.M., Tsai, C.H. and Li, H.
45
46 (2000) A mouse model for spinal muscular atrophy. *Nat. Genet.*, **24**, 66–70.
47
48
- 49 23. Huang, D.W., Sherman, B.T. and Lempicki, R.A. (2009) Systematic and integrative
50
51 analysis of large gene lists using DAVID bioinformatics resources. *Nat. Protoc.*, **4**, 44–
52
53 57.
54
55
- 56 24. Huang, D.W., Sherman, B.T. and Lempicki, R.A. (2009) Bioinformatics enrichment
57
58 tools: paths toward the comprehensive functional analysis of large gene lists. *Nucleic*
59
60

- 1
2
3 *Acids Res.*, **37**, 1–13.
4
5
6 25. Szklarczyk, D., Franceschini, A., Wyder, S., Forslund, K., Heller, D., Huerta-Cepas, J.,
7 Simonovic, M., Roth, A., Santos, A., Tsafou, K.P., *et al.* (2015) STRING v10: protein–
8 protein interaction networks, integrated over the tree of life. *Nucleic Acids Res.*, **43**.
9
10
11
12 26. Fuller, H.R., Gillingwater, T.H. and Wishart, T.M. (2016) Commonality amid diversity:
13 Multi-study proteomic identification of conserved disease mechanisms in spinal
14 muscular atrophy. *Neuromuscul. Disord.*, **26**, 560–569.
15
16
17
18
19 27. Mutsaers, C.A., Lamont, D.J., Hunter, G., Wishart, T.M. and Gillingwater, T.H. (2013)
20 Label-free proteomics identifies Calreticulin and GRP75/Mortalin as peripherally
21 accessible protein biomarkers for spinal muscular atrophy. *Genome Med*, **5**.
22
23
24
25
26 28. Aghamaleky Sarvestany, A., Hunter, G., Tavendale, A., Lamont, D.J., Hurtado, M.L.,
27 Graham, L.C., Wishart, T.M. and Gillingwater, T.H. (2014) Label-Free Quantitative
28 Proteomic Profiling Identifies Disruption of Ubiquitin Homeostasis As a Key Driver of
29 Schwann Cell Defects in Spinal Muscular Atrophy. *J. Proteome Res.*, **13**, 4546–4557.
30
31
32
33
34
35 29. Fuller, H.R., Mandefro, B., Shirran, S.L., Gross, A.R., Kaus, A.S., Botting, C.H., Morris,
36 G.E. and Sareen, D. (2016) Spinal Muscular Atrophy Patient iPSC-Derived Motor
37 Neurons Have Reduced Expression of Proteins Important in Neuronal Development.
38 *Front. Cell. Neurosci.*, **9**, 506.
39
40
41
42
43
44 30. Le Dour, C., Macquart, C., Sera, F., Homma, S., Bonne, G., Morrow, J.P., Worman, H.J.
45 and Muchir, A. (2017) Decreased WNT/b-catenin signalling contributes to the
46 pathogenesis of dilated cardiomyopathy caused by mutations in the lamin a/C gene.
47 *Hum. Mol. Genet.*, **26**, 333–343.
48
49
50
51
52
53 31. Bermeo, S., Vidal, C., Zhou, H. and Duque, G. (2015) Lamin A/C Acts as an Essential
54 Factor in Mesenchymal Stem Cell Differentiation Through the Regulation of the
55 Dynamics of the Wnt/ β -Catenin Pathway. *J. Cell. Biochem.*, **116**, 2344–2353.
56
57
58
59
60

- 1
2
3 32. Sullivan, T., Escalante-Alcalde, D., Bhatt, H., Anver, M., Bhat, N., Nagashima, K.,
4
5 Stewart, C.L. and Burke, B. (1999) Loss of A-type Lamin Expression Compromises
6
7 Nuclear Envelope Integrity Leading to Muscular Dystrophy. *J. Cell Biol.*, **147**, 913–919.
8
9
10 33. Kubben, N., Voncken, J.W., Demmers, J., Calis, C., van Almen, G., Pinto, Y. and Misteli,
11
12 T. (2010) Identification of differential protein interactors of lamin A and progerin.
13
14 *Nucleus*, **1**, 513–525.
15
16
17 34. Ramser, J., Ahearn, M.E., Lenski, C., Yariz, K.O., Hellebrand, H., von Rhein, M., Clark,
18
19 R.D., Schmutzler, R.K., Lichtner, P., Hoffman, E.P., *et al.* (2008) Rare Missense and
20
21 Synonymous Variants in UBE1 Are Associated with X-Linked Infantile Spinal
22
23 Muscular Atrophy. *Am. J. Hum. Genet.*, **82**, 188–193.
24
25
26 35. Antonellis, A., Ellsworth, R.E., Sambuughin, N., Puls, I., Abel, A., Lee-Lin, S.-Q.,
27
28 Jordanova, A., Kremensky, I., Christodoulou, K., Middleton, L.T., *et al.* (2003) Glycyl
29
30 tRNA synthetase mutations in Charcot-Marie-Tooth disease type 2D and distal spinal
31
32 muscular atrophy type V. *Am. J. Hum. Genet.*, **72**, 1293–1299.
33
34
35 36. Sivakumar, K., Kyriakides, T., Puls, I., Nicholson, G.A., Funalot, B., Antonellis, A.,
36
37 Sambuughin, N., Christodoulou, K., Beggs, J.L., Zamba-Papanicolaou, E., *et al.* (2005)
38
39 Phenotypic spectrum of disorders associated with glycyl-tRNA synthetase mutations.
40
41 *Brain*, **128**, 2304–2314.
42
43
44 37. James, P.A., Cader, M.Z., Muntoni, F., Childs, A.-M., Crow, Y.J. and Talbot, K. (2006)
45
46 Severe childhood SMA and axonal CMT due to anticodon binding domain mutations in
47
48 the GARS gene. *Neurology*, **67**, 1710–2.
49
50
51 38. Naetar, N., Ferraioli, S. and Foisner, R. (2017) Lamins in the nuclear interior – life
52
53 outside the lamina. *J. Cell Sci.*, **130**, 2087–2096.
54
55
56 39. Harada, T., Swift, J., Irianto, J., Shin, J.W., Spinler, K.R., Athirasala, A., Diegmiller, R.,
57
58 Dingal, P.C.D.P., Ivanovska, I.L. and Discher, D.E. (2014) Nuclear lamin stiffness is a
59
60

- 1
2
3 barrier to 3D migration, but softness can limit survival. *J. Cell Biol.*, **204**, 669–682.
4
5
6 40. Swift, J., Ivanovska, I.L., Buxboim, A., Harada, T., Dingal, P.C.D.P., Pinter, J.,
7
8 Pajeroski, J.D., Spinler, K.R., Shin, J.-W., Tewari, M., *et al.* (2013) Nuclear Lamin-A
9
10 Scales with Tissue Stiffness and Enhances Matrix-Directed Differentiation. *Science*,
11
12 **341**, 965–966.
13
14
15 41. Borbély, A., Van Der Velden, J., Papp, Z., Bronzwaer, J.G.F., Edes, I., Stienen, G.J.M.
16
17 and Paulus, W.J. (2005) Cardiomyocyte Stiffness in Diastolic Heart Failure. *Circulation*,
18
19 **111**, 774–781.
20
21
22 42. Røe, A.T., Magnus Aronsen, J., Skårdal, K., Hamdani, N., Linke, W.A., Danielsen, H.E.,
23
24 Sejersted, O.M., Sjaastad, I. and Louch, W.E. (2017) Increased passive stiffness
25
26 promotes diastolic dysfunction despite improved Ca²⁺ handling during left ventricular
27
28 concentric hypertrophy. *Cardiovasc. Res.*, **113**, 1161–1172.
29
30
31 43. Lanzicher, T., Martinelli, V., Puzzi, L., Del Favero, G., Codan, B., Long, C.S., Mestroni,
32
33 L., Taylor, M.R.G. and Sbaizero, O. (2015) The Cardiomyopathy Lamin A/C D192G
34
35 Mutation Disrupts Whole-Cell Biomechanics in Cardiomyocytes as Measured by
36
37 Atomic Force Microscopy Loading-Unloading Curve Analysis. *Sci. Reports*, **5**.
38
39
40 44. Heier, C.R., Satta, R., Lutz, C. and Didonato, C.J. (2010) Arrhythmia and cardiac defects
41
42 are a feature of spinal muscular atrophy model mice. *Hum. Mol. Genet.*, **19**, 3906–3918.
43
44
45 45. Bogdanik, L.P., Osborne, M.A., Davis, C., Martin, W.P., Austin, A., Rigo, F., Frank
46
47 Bennett, C. and Lutz, C.M. (2015) Systemic, postsymptomatic antisense oligonucleotide
48
49 rescues motor unit maturation delay in a new mouse model for type II/III spinal
50
51 muscular atrophy. *PNAS*, **112**, E5863–E5872.
52
53
54 46. Shababi, M., Habibi, J., Ma, L., Glascock, J.J., Sowers, J.R. and Lorson, C.L. (2012)
55
56 Partial restoration of cardio-vascular defects in a rescued severe model of spinal
57
58 muscular atrophy. *J. Mol. Cell. Cardiol.*, **52**, 1074–1082.
59
60

- 1
2
3
4
5
6
7
8
9
10
11
12
13
14
15
16
17
18
19
20
21
22
23
24
25
26
27
28
29
30
31
32
33
34
35
36
37
38
39
40
41
42
43
44
45
46
47
48
49
50
51
52
53
54
55
56
57
58
59
60
47. Yasuma, F., Kuru, S. and Konagaya, M. (2004) Dilated Cardiomyopathy in Kugelberg-Welander Disease: Coexisting Sleep Disordered Breathing and Its Treatment with Continuous Positive Airway Pressure. *Intern. Med.*, **43**, 951–954.
48. Roos, M., Sarkozy, A., Chierchia, G.B., De Wilde, P., Schmedding, E. and Brugada, P. (2009) Malignant Ventricular Arrhythmia in a Case of Adult Onset of Spinal Muscular Atrophy (Kugelberg-Welander Disease). *J Cardiovasc Electrophysiol*, **20**, 342–344.
49. Le Dour, C., Wu, W., Béréziat, V., Capeau, J., Vigouroux, C. and Worman, H.J. (2017) Extracellular matrix remodeling and transforming growth factor- β signaling abnormalities induced by lamin A/C variants that cause lipodystrophy. *J. Lipid Res.*, **58**, 151–163.
50. van Tintelen, J.P., Tio, R.A., Kerstjens-Frederikse, W.S., van Berlo, J.H., Boven, L.G., Suurmeijer, A.J.H., White, S.J., den Dunnen, J.T., te Meerman, G.J., Vos, Y.J., *et al.* (2007) Severe Myocardial Fibrosis Caused by a Deletion of the 5' End of the Lamin A/C Gene. *J. Am. Coll. Cardiol.*, **49**, 2430–2439.
51. Taranum, S., Vaylann, E., Meinke, P., Abraham, S., Yang, L., Neumann, S., Karakesisoglou, I., Wehnert, M. and Noegel, A.A. (2012) LINC complex alterations in DMD and EDMD/CMT fibroblasts. *Eur. J. Cell Biol.*, **91**, 614–628.
52. Zahr, H.C. and Jaalouk, D.E. (2018) Exploring the Crosstalk Between LMNA and Splicing Machinery Gene Mutations in Dilated Cardiomyopathy. *Front. Genet*, **9**.
53. Meinke, P., Mattioli, E., Haque, F., Antoku, S., Columbaro, M., Straatman, K.R., Worman, H.J., Gundersen, G.G., Lattanzi, G., Wehnert, M., *et al.* (2014) Muscular Dystrophy-Associated SUN1 and SUN2 Variants Disrupt Nuclear-Cytoskeletal Connections and Myonuclear Organization. *PLoS Genet.*, **10**, e1004605.
54. Szibor, M., Pöling, J., Warnecke, H., Kubin, T. and Braun, T. (2014) Remodeling and dedifferentiation of adult cardiomyocytes during disease and regeneration. *Cell. Mol.*

- 1
2
3 *Life Sci*, **71**, 1907–1916.
4
5
6 55. Communal, C., Sumandea, M., de Tombe, P., Narula, J., Solaro, R.J. and Hajjar, R.J.
7
8 (2002) Functional consequences of caspase activation in cardiac myocytes. *PNAS*, **99**,
9
10 6252–6256.
11
12 56. Riessland, M., Ackermann, B., Forster, A., Jakubik, M., Hauke, J., Garbes, L., Fritzsche,
13
14 I., Mende, Y., Blumcke, I., Hahnen, E., *et al.* (2010) SAHA ameliorates the SMA
15
16 phenotype in two mouse models for spinal muscular atrophy. *Hum. Mol. Genet.*, **19**,
17
18 1492–1506.
19
20
21 57. Fuller, H.R., Hurtado, M.L., Wishart, T.M. and Gates, M.A. (2014) The rat striatum
22
23 responds to nigro-striatal degeneration via the increased expression of proteins
24
25 associated with growth and regeneration of neuronal circuitry. **12**.
26
27
28 58. Šoltić, D., Bowerman, M., Stock, J., Shorrock, H.K., Gillingwater, T.H. and Fuller, H.R.
29
30 (2018) Multi-Study Proteomic and Bioinformatic Identification of Molecular Overlap
31
32 between Amyotrophic Lateral Sclerosis (ALS) and Spinal Muscular Atrophy (SMA).
33
34 *Brain Sci.*, **8**.
35
36
37 59. Young, P.J., Le, T.T., thi Man, N., Burghes, A.H.M. and Morris, G.E. (2000) The
38
39 Relationship between SMN, the spinal muscular atrophy protein, and nuclear coiled
40
41 bodies in differentiated tissues and cultured cells. *Exp. Cell Res.*, **256**, 365–374.
42
43
44 60. Manilal, S., Randles, K.N., Aunac, C., Nguyen, M. thi and Morris, G.E. (2004) A lamin
45
46 A/C beta-strand containing the site of lipodystrophy mutations is a major surface epitope
47
48 for a new panel of monoclonal antibodies. *Biochim. Biophys. Acta*, **1671**, 87–92.
49
50
51 61. Schindelin, J., Arganda-Carreras, I., Frise, E., Kaynig, V., Longair, M., Pietzsch, T.,
52
53 Preibisch, S., Rueden, C., Saalfeld, S., Schmid, B., *et al.* (2012) Fiji: an open-source
54
55 platform for biological-image analysis. *Nat. Methods*, **9**, 676–682.
56
57
58 62. Radonić, A., Thulke, S., Mackay, I.M., Landt, O., Siegert, W. and Nitsche, A. (2004)
59
60

1
2
3 Guideline to reference gene selection for quantitative real-time PCR. *Biochem. Biophys.*
4
5 *Res. Commun.*, **313**, 856–62.
6
7

8 63. Pfaffl, M.W. (2001) A new mathematical model for relative quantification in real-time
9
10 RT-PCR. *Nucleic Acids Res.*, **29**, e45.
11

12 64. Fuller, H.R., Marani, L., Holt, I., Woodhams, P.L., Webb, M.M. and Gates, M.A. (2017)
13
14 Monoclonal antibody Py recognizes neurofilament heavy chain and is a selective marker
15
16 for large diameter neurons in the brain. *Brain Struct. Funct.*, **222**, 867–879.
17
18
19
20
21
22
23
24
25
26
27
28
29
30
31
32
33
34
35
36
37
38
39
40
41
42
43
44
45
46
47
48
49
50
51
52
53
54
55
56
57
58
59
60

For Peer Review

Figure legends

Figure 1. Bioinformatics analysis of the proteins dysregulated in heart tissue from SMA mice. A) Upregulated proteins (n=177) and B) downregulated proteins (n=206) were subjected to STRING 10 analysis. Of these, 103 upregulated and 91 downregulated proteins are not shown as statistically significant interactions were not identified in STRING 10. Protein associations were identified with high confidence (0.700) interaction score for A) upregulated and with the highest confidence (0.900) interaction score for B) downregulated proteins. The thickness and colour of the lines indicate confidence of the interaction (see legend inset in figure). Protein networks were compared to the GO analysis output (Supplementary Table 4). The analysis identified protein clusters that associate with enriched GO terms in the cellular component (black) and biological process (red) domain. Proteins annotated to each term are shown in corresponding circles.

Figure 2. Widespread dysregulation of lamin A/C expression in fibroblasts from SMA patients and in tissues from SMA mice (P8) A) Schematic diagram showing the quantitative western blot analysis workflow. Total protein extracts from human fibroblast cells and mouse tissues were subjected to SDS-PAGE. A part of the gel was stained with Coomassie blue as an internal, total protein loading control. Proteins from the remaining part of the gel were transferred to nitrocellulose membrane and developed with the appropriate antibody. Quantification of protein levels was performed by normalising densitometry measurements of antibody reactive bands to densitometry measurements of Coomassie stained gel. Image created with BioRender.com. B) Representative western blots showing lamin A/C protein levels in the heart, spinal cord, brain, liver and muscle tissue from SMA mice (n=5) and healthy controls (n = 5), and in fibroblast cells from SMA patients (n = 3) and

1
2
3 age matched male healthy controls (n = 3). Fibroblast cells are listed in this order: 1.
4 GM00498, 2. GM05659, 3. GM00302, 4. GM03813, 5. GM09677, 6. GM00232. The
5
6 uncropped blots and total protein loading controls can be found in the Supplementary File
7
8 (S3). C) Quantification of lamin A/C levels in tissues from SMA mice and in patient
9
10 fibroblast cells. In the liver extract, the lower band was presumed to be lamin C, and the
11
12 upper two bands were presumed to be lamin A isoforms and were consequently measured
13
14 together to give a single value. The graph is presented as average protein levels in SMA
15
16 tissues (expressed relative to the control), with error bars showing standard deviation from
17
18 the mean. The dashed line represents protein levels across healthy control tissues. D)
19
20 Representative immunohistochemistry images showing lamin A/C staining in the heart from
21
22 SMA mouse (P8) and healthy age-matched control. Scale bar = 50 μ m. Increased lamin A/C
23
24 staining can be observed in the ventricle wall from SMA mouse, with few lamin A/C positive
25
26 cells found in the ventricle lumen. E) Densitometry measurements of lamin A/C levels in the
27
28 ventricle wall are presented as mean optical density, with error bars showing standard
29
30 deviation from the mean. F) Lamin A transcript levels in the heart from SMA mice (n = 4)
31
32 and healthy controls (n = 4) and in fibroblast cells from SMA patients (n = 3) and healthy
33
34 controls (n = 3). Expression levels of lamin A were normalized to the geometric mean of
35
36 *POLR2J* and *TBP*. The graphs are presented as mean expression, with error bars showing
37
38 standard deviation from the mean. CTR- control; ns—not significant; * p < 0.05; ** p < 0.01;
39
40 *** p < 0.001.
41
42
43
44
45
46
47
48
49
50

51 **Figure 3. UBA1 and lamin A/C are mechanistically linked**

52 Western blots showing lamin A/C, UBA1 and SMN protein levels in the A) heart, muscle,
53
54 liver, brain and spinal cord tissue from healthy control mice (n=2) and in fibroblast cells from
55
56 healthy individuals (n=2), in B) UBA1 KD and control HEK cells (n = 3) and in C) *LMNA*
57
58
59
60

1
2
3 KO and wild type MEFs (n = 3). The uncropped blots and loading controls can be found in
4 the Supplementary File (S5 and S6). Graphs are presented as average protein levels
5 (expressed relative to the control), with error bars showing standard deviation from the mean.
6
7 The dashed line represents protein levels in control cells. H-heart; M-muscle; L-liver; B-
8 brain; SP-spinal cord; FC-fibroblast cells; ns—not significant; *p < 0.05; ** p < 0.01; *** p
9 < 0.001.
10
11
12
13
14
15
16
17
18

19 **Figure 4. Lamin A/C interacts with β -catenin in mouse heart**

20
21 A) Representative immunocytochemistry images showing lamin A and UBA1 staining in
22 control and SMA patient fibroblast cells. Arrows in the lower magnification images indicate
23 cells with the most obvious UBA1 staining at the nuclear periphery. Scale bar = 25 μ m. Scale
24 bar = 10 μ m (control) and 7.5 μ m (SMA) in higher magnification images. B) Western blots
25 showing lamin A/C, UBA1 and β -catenin expression in the heart tissue from control and
26 SMA mice after immunoprecipitation with anti-lamin A/C antibody. Beads alone control
27 lanes refer to heart extracts incubated with Dynabeads without the antibody, and represent
28 negative control. # β -catenin band was detected in the eluate from lamin A/C pulldown in both
29 control and SMA samples, but was not observed in the eluate from the beads alone control.
30
31
32
33
34
35
36
37
38
39
40
41
42
43
44

45 **Figure 5. Model of how lamin A/C dysregulation, in combination with other molecular**
46 **changes, may contribute to cardiac pathology in SMA.** A model is proposed in which
47 lamin A/C up-regulation, in combination with other molecular changes that occur in SMA,
48 may lead to cardiac fibrosis and impaired cardiac function. Thinner ventricle walls and
49 dilated ventricles in SMA heart are clinical features of dilated cardiomyopathy. Image created
50 with BioRender.com.
51
52
53
54
55
56
57
58
59
60

Abbreviations

SMA- spinal muscular atrophy

SMN- survival of motor neuron

SMN1- survival of motor neuron 1, telomeric

SMN2- survival of motor neuron 2, centromeric

LMNA- lamin A/C

ECG- electrocardiogram

iTRAQ- isobaric tags for relative and absolute quantitation

DAVID- database for annotation, visualization and integrated discovery

STRING 10- search tool for the retrieval of interacting genes/proteins

GO- gene ontology

P8-postnatal day 8

RT-qPCR- reverse transcription- quantitative polymerase chain reaction

C_t- cycle threshold

HEK cells - human embryonic kidney cells

MEFs- mouse embryonic fibroblasts

UBA1- ubiquitin like modifier activating enzyme 1

GARS1- glycyl-tRNA synthetase 1

SMA2- spinal muscular atrophy, x-linked 2

MSCs- mesenchymal stem cells

SUN2- SUN domain-containing protein 2

SUN2- Sad1 and UNC84 domain containing 2

Cdc5l- cell division cycle 5-like protein

RPLC- reverse-phase liquid chromatography

LC-ESI-MS/MS - liquid chromatography-tandem mass spectrometry

1
2
3 OD- optical density

4
5 FA- formic acid

6
7
8 DDA- data-dependent acquisition

9
10 CE- collision energy

11
12 FDR- false discovery rate

13
14 PSPEP- Proteomics System Performance Evaluation Pipeline

15
16 DMEM- Dulbecco's Modified Eagle Medium

17
18 FBS- fetal bovine serum

19
20 MEM-NEAA- non-essential amino acids

21
22 PEN-STREP- penicillin-streptomycin

23
24 KD- knockdown

25
26 KO- knockout

27
28 SDS-PAGE- sodium dodecyl sulfate- polyacrylamide gel electrophoresis

29
30 BSA- bovine serum albumin

31
32 PBS- phosphate-buffered saline

33
34 NTC- no-template control

35
36 *POLR2J*- RNA polymerase II subunit J

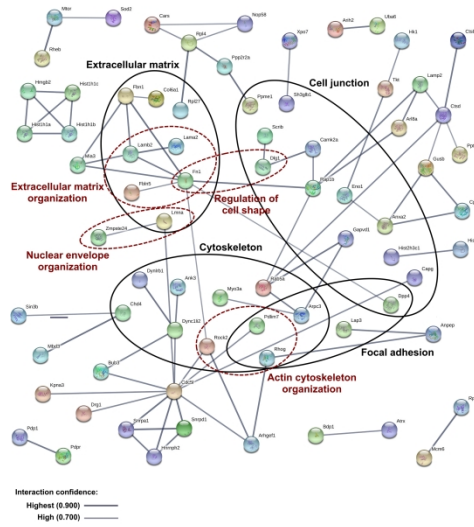
37
38 *TBP*- TATA-Box binding protein

39
40 OCT- optimum cutting temperature compound

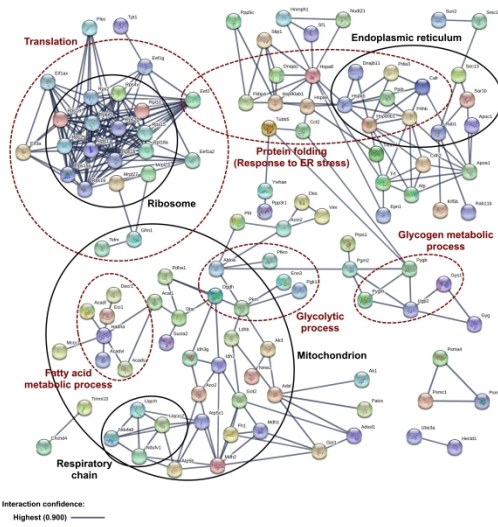
41
42 DAPI- 4',6-diamidino-2-phenylindole

43
44
45
46
47
48
49
50
51
52
53
54
55
56
57
58
59
60

A) Upregulated proteins



B) Downregulated proteins



261x146mm (600 x 600 DPI)

1
2
3
4
5
6
7
8
9
10
11
12
13
14
15
16
17
18
19
20
21
22
23
24
25
26
27
28
29
30
31
32
33
34
35
36
37
38
39
40
41
42
43
44
45
46
47
48
49
50
51
52
53
54
55
56
57
58
59
60

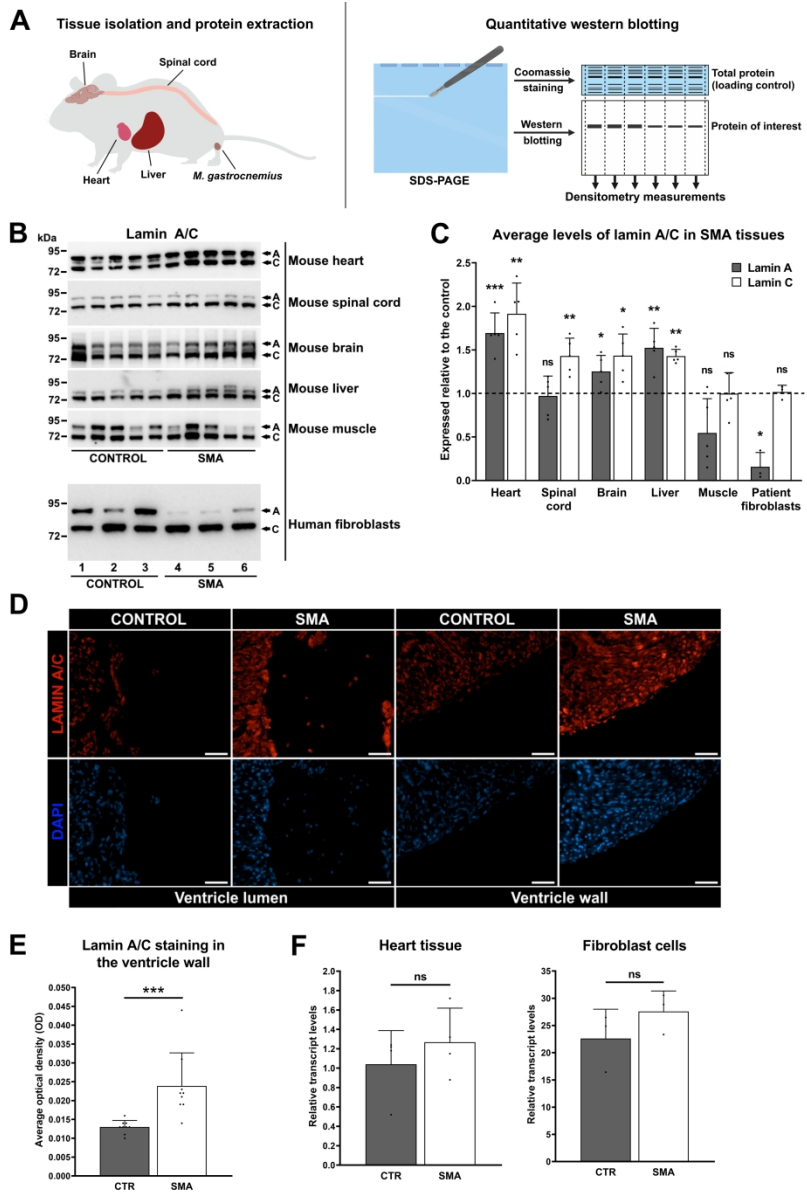


Figure 2

150x223mm (600 x 600 DPI)

1
2
3
4
5
6
7
8
9
10
11
12
13
14
15
16
17
18
19
20
21
22
23
24
25
26
27
28
29
30
31
32
33
34
35
36
37
38
39
40
41
42
43
44
45
46
47
48
49
50
51
52
53
54
55
56
57
58
59
60

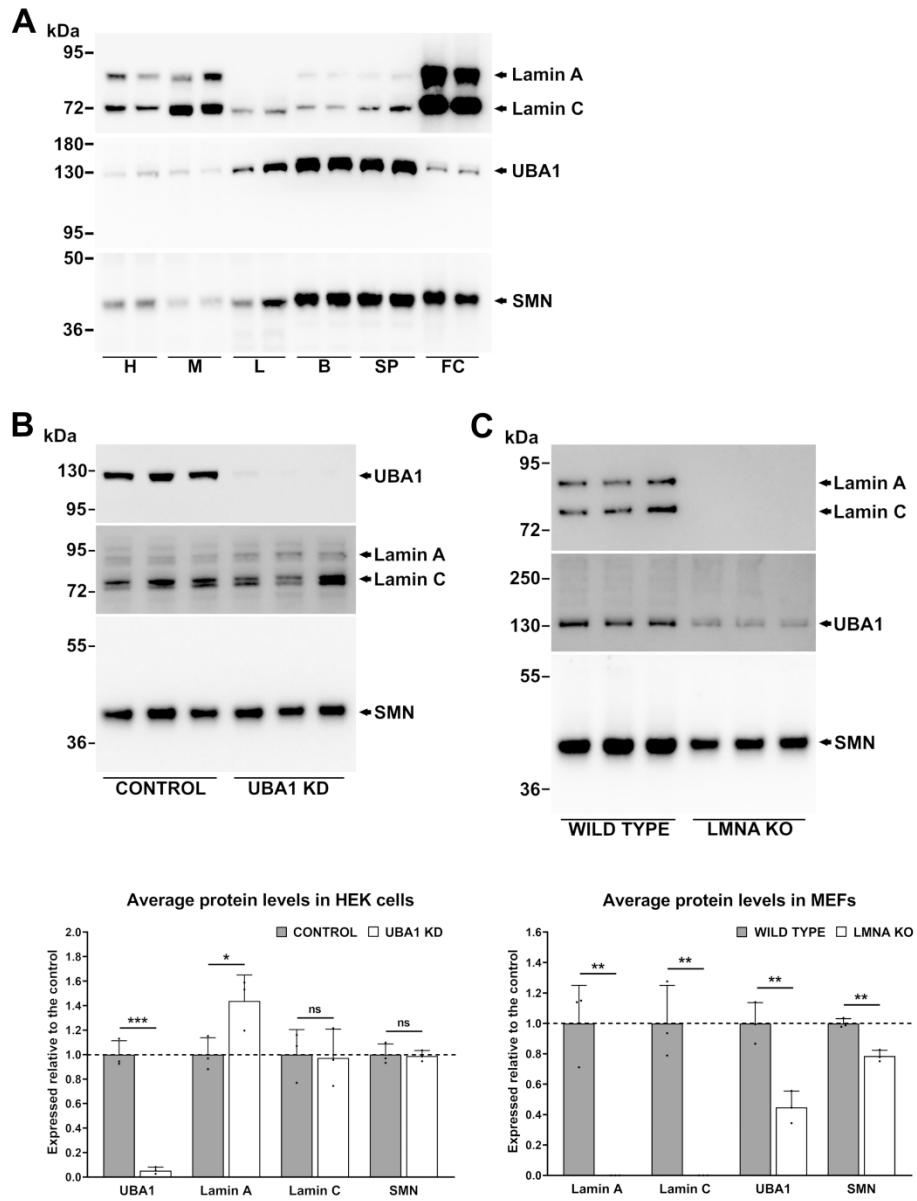


Figure 3

142x186mm (600 x 600 DPI)

1
2
3
4
5
6
7
8
9
10
11
12
13
14
15
16
17
18
19
20
21
22
23
24
25
26
27
28
29
30
31
32
33
34
35
36
37
38
39
40
41
42
43
44
45
46
47
48
49
50
51
52
53
54
55
56
57
58
59
60

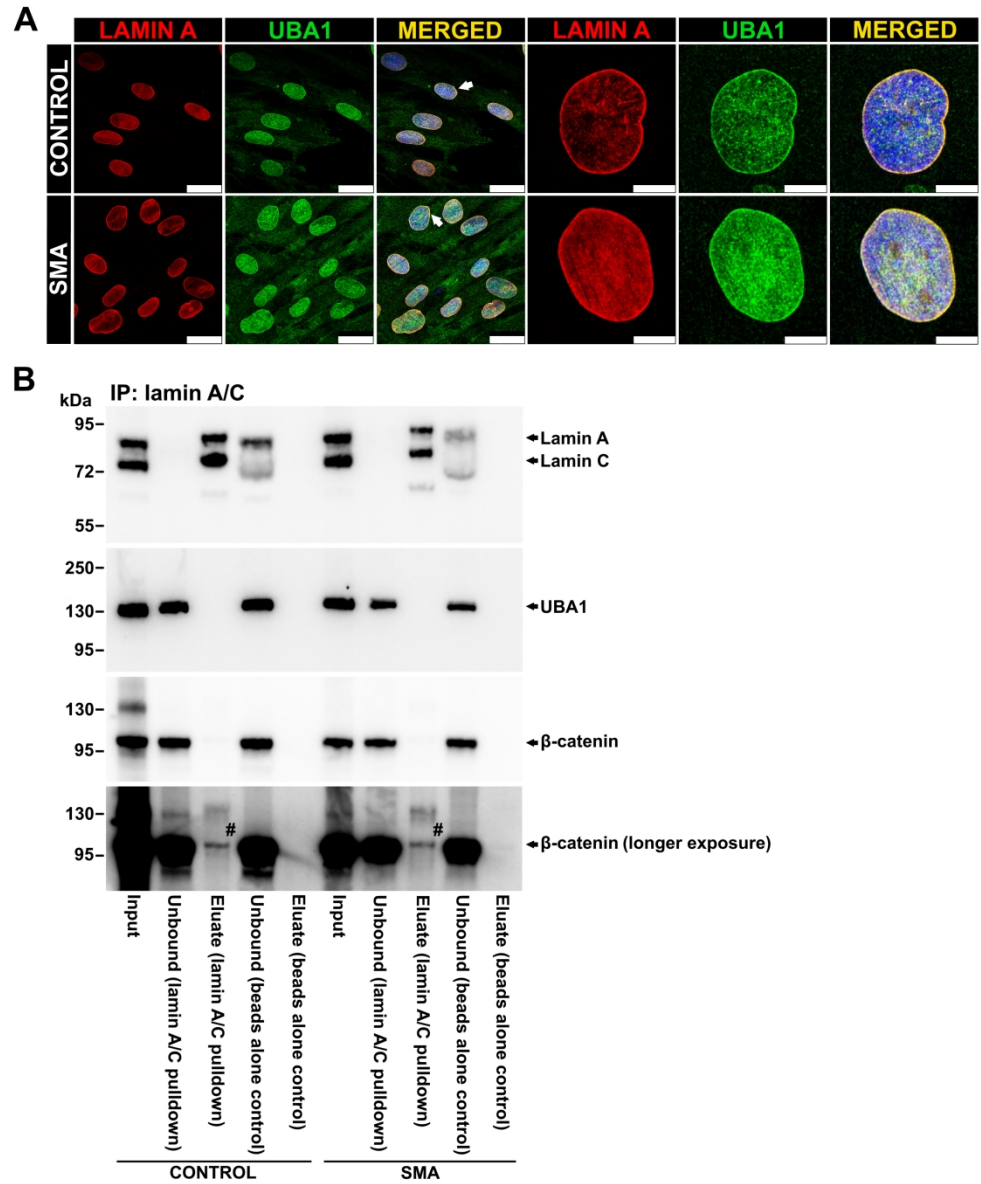


Figure 4

154x188mm (600 x 600 DPI)

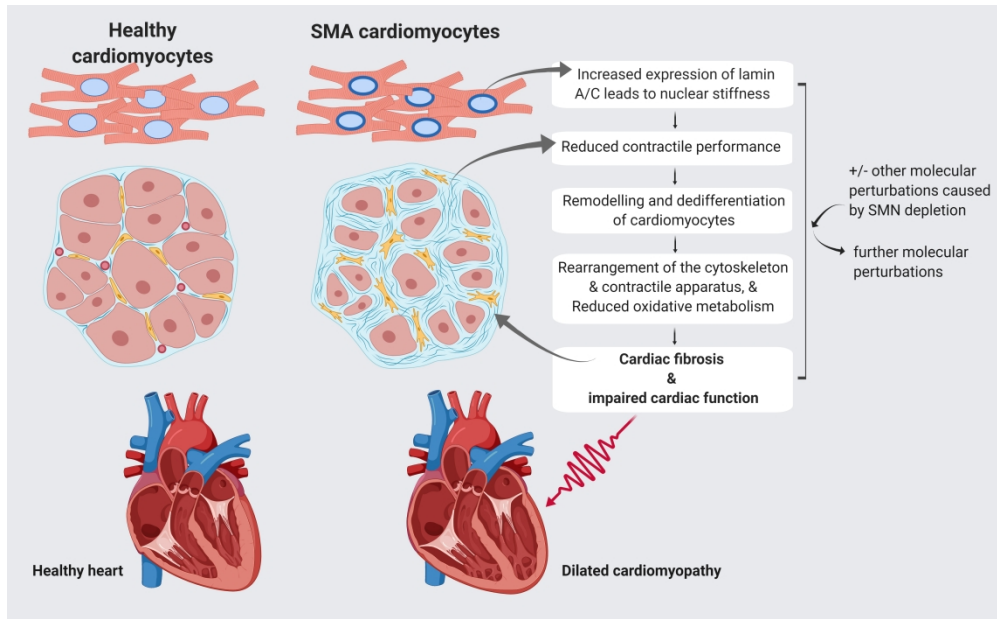


Figure 5